ELSEVIER_TECTO_126344

Scaling, kinematics and evolution of a polymodal fault system: Hail Creek Mine, NE Australia

Jacob Carvell[a]

Thomas Blenkinsop[a, b, *]

BlenkinsopT@Cardiff.ac.uk

Gavin Clarke[a]

Maurizio Tonelli[c]

[a]Economic Geology Research Unit, School of Earth and Environmental Science, James Cook University, ~~Queensland~~ QLD 4811, Australia

[b]School of Earth and Ocean Science, Cardiff University, Main Building, Park Place, Cardiff CF10 3AT, United Kingdom

[c]Hail Creek Coal Mine, PO Box 3097, North Mackay, QLD 4740, Australia

*Corresponding author at: School of Earth and Ocean Science, Cardiff University, Main Building, Park Place Cardiff CF10 3AT, United Kingdom. Tel.: + 44 29 208 70232.

Abstract

We analyse a system of normal faults that ~~cut~~ cuts sandstone~~s~~, siltstone~~s~~, mudstone, coal, and tuff at Hail Creek Coal Mine in the Bowen Basin, NE Australia. Our detailed mapping ~~utilized~~ utilised the dense borehole network and strip mining operations. The fault surfaces have complex geometries, yet the components of the individual faults show similar orientation variability to the whole fault system. The faults and their components dip to the SE, NW, NNW, and SSE with an orthorhombic symmetry that we refer to as polymodal. There are multiple displacement peaks, with complementary changes on adjacent faults. This observation suggests kinematic coherence between neighbouring faults. Twin displacement peaks on some faults suggest that segment linkage occurred on a scale of hundreds of m. These polymodal faults follow the same displacement~~–~~–length scaling laws as other normal faults. Fault dip is affected by lithology, with steeper dips in more competent (sandstone) beds. An 'odd axis' construction using whole fault planes suggests that they formed in a triaxial strain state (three different principal strains) with vertical shortening, and horizontal extension along principal directions of 148° and 058°. Odd axis constructions using individual fault components, as opposed to whole faults, give similar principal strain orientations and maximum strain ratios. The variable component orientations, and the consistency of fault kinematics on different scales, suggest that the faults evolved by the propagation or linkage of smaller components with variable orientations, within the same bulk strain state.

Keywords: Normal fault; Orthorhombic fault; Polymodal fault; Displacement~~–~~–length scaling; Coal; Mine

1 Introduction

Polymodal fault systems are sets of faults in three or more orientations that formed in relation to a common state of strain. The importance of polymodal fault systems was first demonstrated by Oertel (1965) in a series of remarkable experiments on clay deformed in a three-dimensional strain state, including measurements of both displacements and stress. He outlined a theoretical framework for the development of four sets of faults, which were related to the principal strain rate axes by symmetry arguments and tensor geometry. Oertel~~'~~s work was followed up a decade later by Reches (1978, 1983), Aydin and Reches (1982) and Reches and Dieterich (1983), who produced field and experimental evidence for polymodal fault sets, and analysed the strain associated with their formation. Krantz (1988) documented polymodal faults and showed how strain states could be inferred from field measurements by the "Odd Axis" method. Subsequently, Healy et al. (2006a, b) drew attention to the existence of non-Andersonian, polymodal fault sets, and proposed a model for their formation based in crack tip interactions. Fig. 1 displays the differences between conjugate faults predicted by Andersonian fault theory, and a polymodal fault geometry.

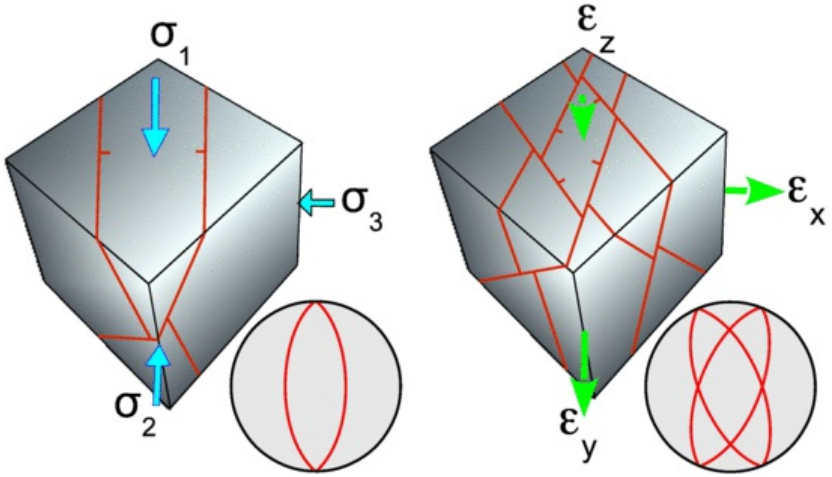

Fig. 1 Differences between Andersonian faults (left) and orthorhombic fault systems (right), illustrated for normal faults. Equal area, lower hemisphere stereoplots in each case show fault plane orientations (great circles). Andersonian faults are conjugate faults symmetrical about the principal stresses ($\sigma_1 \geq \sigma_2 \geq \sigma_3$, compression positive) (Anderson, 1951). Orthorhombic faults systems have four orientations symmetrical about the principal strains ($\varepsilon_x \geq \varepsilon_y \geq \varepsilon_z$, elongation positive) (cf. Reches, 1978).

Independently of work on polymodal faults, fault scaling relationships between parameters such as length and displacement were established (Barnett et al., 1987; Cladouhos and Marrett, 1996; Clark and Cox, 1996; Cowie and Scholz, 1992a,b; Dawers et al., 1993; Muraoka and Kamata, 1983; Peacock, 2002; Walsh and Watterson, 2002; Walsh et al., 2002; Watterson, 1986). These studies revealed a power law equation: $d_{max} = cL^n$ for ~~displacement~~ displacement–length distributions, where d_{max} = ~~–~~maximum cumulative displacement, L = maximum linear dimension, c = a scaling parameter, and n = an exponent in the range of 0.5 to 2. The vicissitudes of this exercise have been comprehensively summarised by Kim and Sanderson (2005), who have concluded that displacement–length scaling depends on material property, type of fault, earthquake rupture and slip/propagation history, fault network evolution and reactivation.

Displacement–length scaling relationships have been interpreted or predicted by (a) individual fault growth models (e.g. Cowie and Scholz, 1992a,b; Marrett and Allmendinger, 1991; Walsh and Watterson, 1987; Walsh et al., 2002; Watterson, 1986); and (b) models for how fault systems evolve through hard and soft linkage (e.g. Barnett et al., 1987; Cartwright et al., 1995; Dawers and Anders, 1995; Nicol et al., 1996; Peacock and Sanderson, 1991; Schilsche, 1992; Walsh and Watterson, 1991). These studies have demonstrated the importance of mapping displacement distributions along line profiles and particularly over the whole fault surface. The latter has usually only been achieved through the analysis of offshore seismic reflection data (e.g. Alves, 2012; Nicol et al., 2005).

Studies of fault scaling, fault displacement accumulation and fault interaction have not addressed the formation or evolution of polymodal fault systems. It is not known, for example, if faults belonging to polymodal sets follow the same scaling laws as other faults, whether displacement exchange may occur between faults in a polymodal system, or how such systems evolve. The goal of the present study is to address these problems.

We document the polymodal fault system at Hail Creek open-strip coal mine in Queensland, Australia. The example is excellent for investigating in detail the geometry, fault scaling relationships, kinematics and evolution of such a system. The strip mining and the large drilling and mining database at Hail Creek provide detailed information about the geometry and displacements of the faults, giving insights into the evolution of the fault system.

2 Geological background

2.1 Stratigraphic context

The coal seams exploited at Hail Creek Mine are part of the Rangal Coal Measures, within the Bowen Basin (Fig. 2). The Rangal Coal Measures formed in the Late Permian as cold climate alluvial coal systems (Michaelsen and Henderson, 2000). They are ~~characterized~~ characterised by immature volcaniclastic sediments and coal. At Hail Creek, the Coal Measures contain two distinct coal seams, locally called the Elphinstone and the Hynds seam, which are on average 6 and 8 m thick respectively, and are separated by up to 30 m of interbedded sandstone, siltstone, mudstone, and tuff. Deposition of the Rangal Coal Measures occurred when the Bowen Basin was in a state of foreland loading (Michaelsen and Henderson, 2000). The Rangal Coal Measures mark the end of the Permian, and are overlain by the Triassic Rewan Group. The contact between these two units is considered to be the Permian–Triassic boundary.

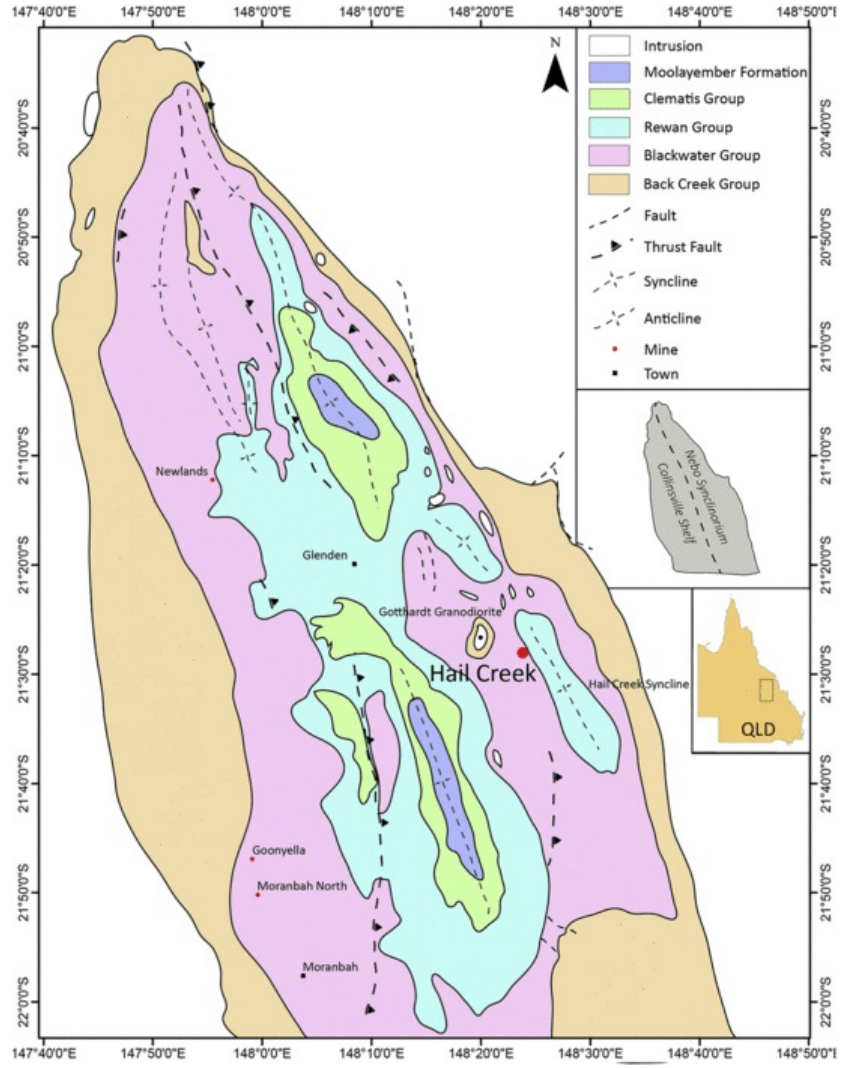

Fig. 2 Geological setting of Hail Creek Coal Mine in the Nebo Synclinorium, Bowen Basin, showing the doubly plunging folds and thrust faults. Adapted from Mallet et al. (1995).

2.2 Structural features of the Northern Bowen Basin

Mallet et al. (1995) divided the northern Bowen Basin into two major morpho-tectonic divisions: the Collinsville Shelf and the Nebo Synclinorium. The Collinsville Shelf is a weakly deformed terrane that bounds the Nebo Synclinorium to the W, with ~~localized~~ localised thrusting along its eastern side (Mallet et al., 1995). The Hail Creek Mine is situated on the western limb of the Hail Creek Syncline, which is an eastern part of the Nebo Synclinorium (Fig. 2). The synclinorium is a fold and thrust belt ~~characterized~~ characterised by open, doubly plunging fold structures and common strike-slip and reverse faults (Fig. 2). The eastern margin comprises generally moderately W dipping strata, disrupted by dense faulting, principally of large scale thrust faults and strike-slip faults (Mallet et al., 1995). The western side of the synclinorium generally dips moderately to the E, with thrust faults being the most prominent structural features (Mallet et al., 1995). Thrust faults most commonly strike N to NW, and are cross-cut by high angle strike slip faults (Esterle et al., 2002).

The Hail Creek Syncline trends NW–SE, and closes to the NW and SE (Fig. 2). Mallet et al. (1995) suggest that this structure was formed during major E–W shortening in the middle Triassic. Thrust faults with throws from a few cm to over three m offset the coal seams at Hail Creek, as exposed in the high wall. The thrusts generally dip at angles of 20°–30°, towards the NE in the NW part of the syncline, and to the SW on the eastern side of the syncline. Similar thrust faults are evident throughout the northern Bowen

Basin (Korsch et al., 1992, 2009; Michaelsen and Henderson, 2000).

The most prominent faults exposed at the Hail Creek Mine, however, are normal faults (Fig. 3). The throw on these faults varies from less than 1 m to 32 m. The faults dip moderately—steeply to the SE, NW, NNW, and SSE, and they cross-cut all the phases of intrusion and the thrust faulting described above. Malone et al. (1991) concluded that since the youngest local basaltic intrusions are Tertiary in age (Sutherland, 1978), the normal faults have a maximum Tertiary age.

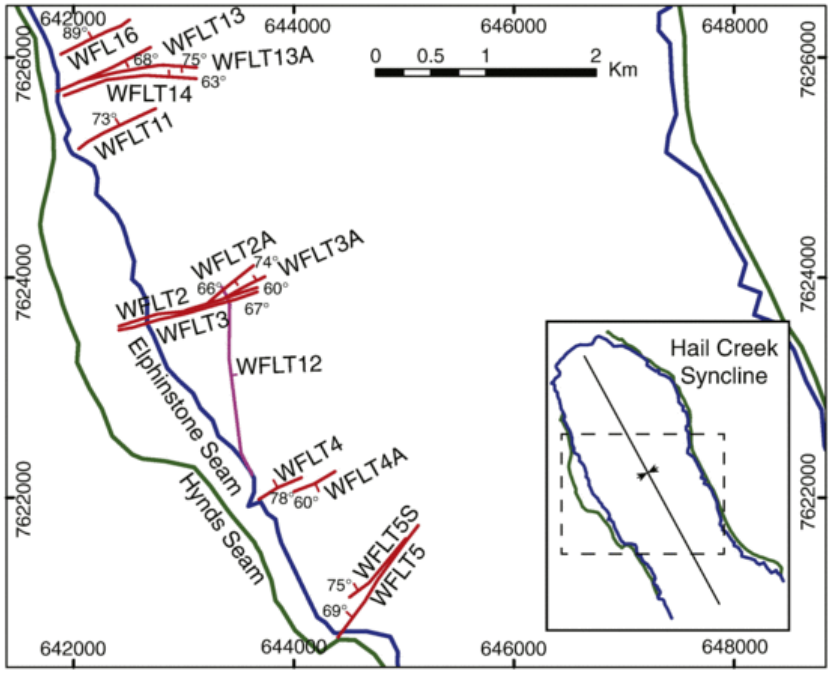

Fig. 3 Map of the faults examined at Hail Creek Coal Mine. The normal faults are grouped into four clusters of two to four faults, with average fault dips varying from 60° to 89°. Faults dip in four directions: SE, NW, NNW, and SSE, constituting a polymodal set.

3 Data and methods

The study area was confined to the section of the Hail Creek Syncline located in Rio Tinto's tenement (Fig. 3). Thirteen normal faults and one thrust fault that have intersected the mine high walls were studied. The faults are named in order of their discovery and by the area of the syncline in which they are located. For example, West Fault 2 (WFLT2) was the second fault to be discovered on the western side of the mine. Seven of the faults (WFLT2A, WFLT3A, WFLT4, WFLT5, WFLT11, WFLT12 and WFLT16) intersected the active high wall in April 2012, where they were sketched and photographed. A total of 8008 drillholes (spacing 76 m) with lithology logs, down-hole geophysical logs, and seam picks have been analysed for this study, covering an area of 72 km^2. Three-dimensional laser scan images of the mine high walls (typically 30 m high) provide centimetre scale resolution on the locations of faults: such images were available from seven positions of the high walls. An extensive photographic record of the walls was also utilised.

A 3-dimensional goCAD model of the faults and coal seams was created covering an area of 27 km^2. Fault surfaces were generated using a combination of drillhole intersections and laser scan point data. Connections between separate points on fault surfaces were inferred from photographs of the pit walls to create fault surfaces as a network of triangles. Coal seam surfaces were constructed from the drillhole data by direct triangulation, and provided controls on fault displacements. Displacements were generated from the seam data using interpolation by kriging, allowing the displacements to be mapped in great detail. The location of some fault tip lines are is known to be within 76 m from the drilling data base and pit mapping, but the full extent of other faults is uncertain. The extremities of the modelled fault surfaces were determined as the outermost drillhole intersection, i.e., no extrapolation of the fault surfaces has been made in the fault surface models. In some cases the coal seam model provided an approximate location of the tip line from observations of offsets in the interpolated coal seams. The dimensions of faults are therefore constrained where possible by intersections with another fault, drilling, or modelling.

The displacements on fault surfaces at Hail Creek Mine were generated at discontinuous points in the kriging process. In order to make a continuous representation, the maximum displacements from strike intervals of approximately 25 m have been selected and joined in a profile. A combined profile of displacement has been produced for each fault group. Since faults within each group dip in opposite directions, the combined profile represents the sum of the absolute value of the

displacements, and does not show the net displacement from one side of the fault group to the other.

Kinematics of the normal faults have ~~has~~ been analysed by the odd axis construction (Krantz, 1988). The odd axis construction is similar to the M-plane method of Arthaud (1969), in which the orientations of the principal strains $\varepsilon_X \geq \varepsilon_Y \geq \varepsilon_Z$, and their ratios, are given by the geometry of the planes linking the pole to slip surfaces and their slip direction (movement planes). Except for the thrust fault, the coal seams have normal separations on all faults over their entire surfaces, and have been assumed to be purely dip slip; there is no evidence suggesting any horizontal component of slip, or of reactivation. Odd axis constructions have been performed for the best fit plane for each fault, as well as for the dip and dip directions extracted from the triangles that make up the model of each fault, as explained in detail below.

4 Individual fault descriptions

The high wall intersects the faults at a median angle of 82° (Table 1), and thus the apparent dips and dip separations of the faults in sketches and photographs (Fig. 4) are very close to the true values. Most faults at Hail Creek have a narrow fault zone (Table 1), with the exception of West Faults 2A, 5 and 13, which have a fault breccia zone up to 3 m wide, between the main fault and a splay. Dip separations range from 0.5 m to 25 m, with an average of 9 m (Table 1). Generally the fault dip varies from 60°–70° in the sandstone units to 40°–50° in the siltstone and coal units. The only exception is West Fault 3A which appears to steepen in the siltstone. Fig. 5 shows the average true fault dip as measured in different lithologies from the drilling data. The highest average dip occurs in the sandstone units followed by siltstone, ~~claystone/~~mudstone, coal and tuff respectively.

Table 1 Descriptions of faults and fault zones that were visible in the high wall at Hail Creek Coal Mine in April 2012. Dip Sep. is dip separation.

Fault	Fault zone appearance	Dip Sep., m	Dip variation	Strike–section angle
WFLT16	Discrete	0.5	Steep in sandstone Shallow in siltstone	85°
WFLT13	Discrete except between the fault and splay up to 10 m from the intersection	15	No variation	82°
WFLT2	Zone of discrete faults 30 m wide	3	60°–70° sandstone 40°–50° siltstone	85°
WFLT2A	Breccia zone 2–3 m wide	10	No variation visible due to fault breccia	59°
WFLT3A	Discrete	4	65° sandstone 40° siltstone	69°
WFLT4	Discrete	7	60°–70° sandstone 40°–50° siltstone	88°
WFLT5	Breccia zone 2–3 m wide	25	No variation visible due to fault breccia	67°

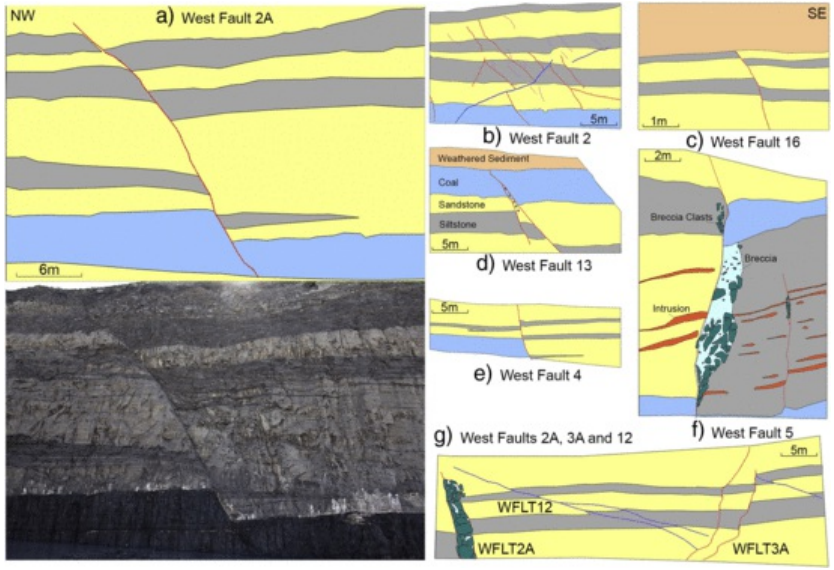

Fig. 4 Sketches and photograph of faults that were visible in the high wall at Hail Creek Coal Mine, April 2012. (a) West Fault 2 with a photograph that shows typical quality of the photographs from which the sketches were made. The fault drawings simplify the strata to emphasise the displacement on the fault. (b) Sketches of other faults as visible on the mine highwall. Light orange—weathered material, yellow—sandstone, grey—siltstone, blue—coal, light blue—breccia, green—breccia clast, and orange—intrusion. Faults are red for normal and blue for thrust faults. (For interpretation of the references to colour in this figure legend, the reader is referred to the web version of this article.)

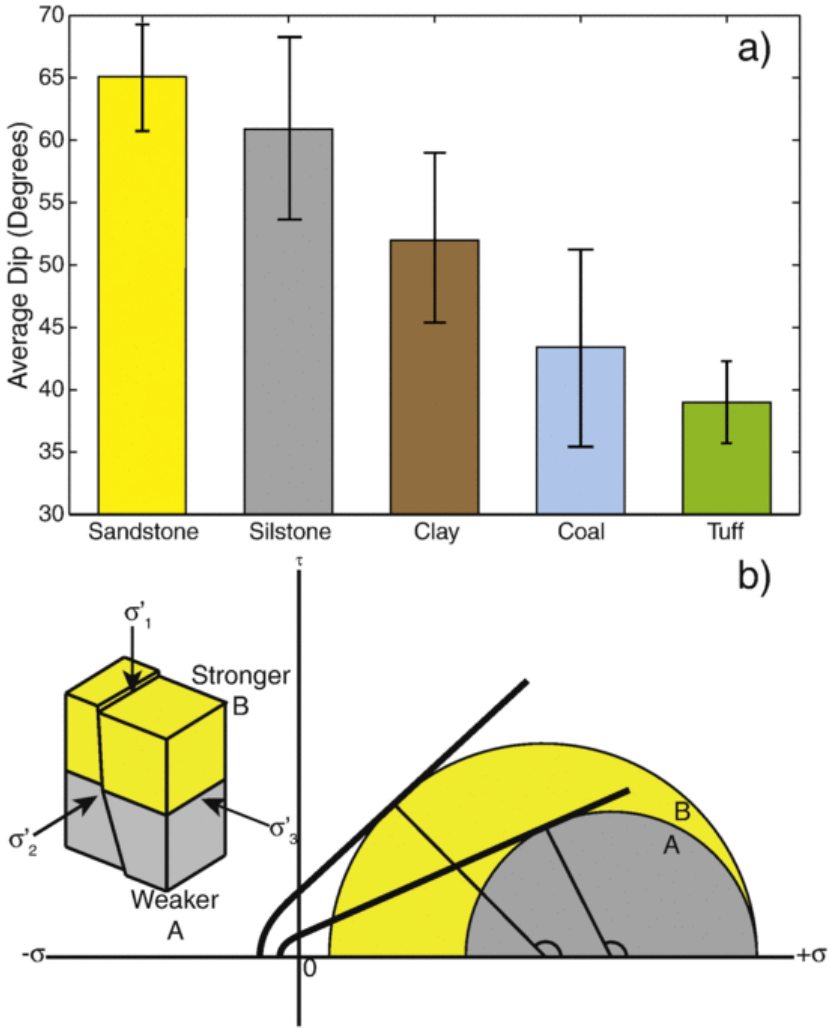

Fig. 5 Fault dip histogram and interpretation on a Mohr Diagram. (a) Average true fault dip (measured in 3-dimensional model of fault surface) by rock type. The more competent rock units have markedly higher average dips. (b) Interpretation of change in fault dip with rock type. A rock such as sandstone with a steeper failure envelop (A) will have a higher angle between fault normal and vertical maximum principal stress at failure and a steeper dip with a vertical maximum principal stress than a weaker one such as siltstone with a less steep failure envelop (B). No particular failure criterion is intended in this diagram. Sandstone and siltstone are used to illustrate the point because they are the most common rock types (Fig. 5).

Displacement–distance graphs have been constructed by plotting all the displacements over the whole surface of each fault (e.g. Fig. 6) at the appropriate horizontal distance from the SW corner of the fault (Fig. 7). The maximum values of the displacement–distance graphs for the Hail Creek faults show characteristics similar to idealised normal faults, as well as to observed fault displacements of coal measures (e.g. Bowring et al., 1998; Finlayson, 1990; Malone et al., 1991). West Fault 4 and West Fault 5 splay (West Fault 5S) show a 'bell curve' distribution across the length of the fault with a maximum displacement in the centre. West Faults 2A and 11 show a skewed shape, with the maximum displacement near one of the tips. The most common pattern is double displacement maxima (West Faults 16, 13A, 13, 12, 5, 4A, and 2).

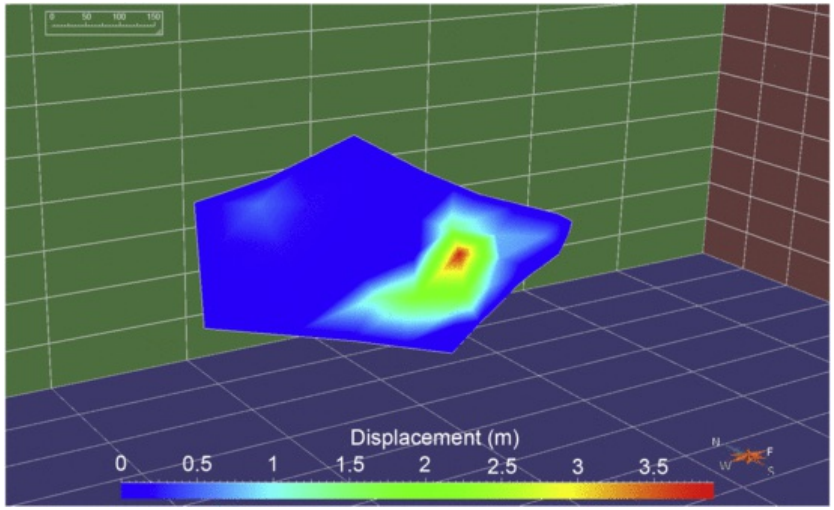

Fig. 6 Screen shot of typical fault surface model coloured by displacement, West Fault 13A. The single displacement maximum is over 4 m. Approximate scale along axes is given in m.

ELSEVIER_TECTO_126344

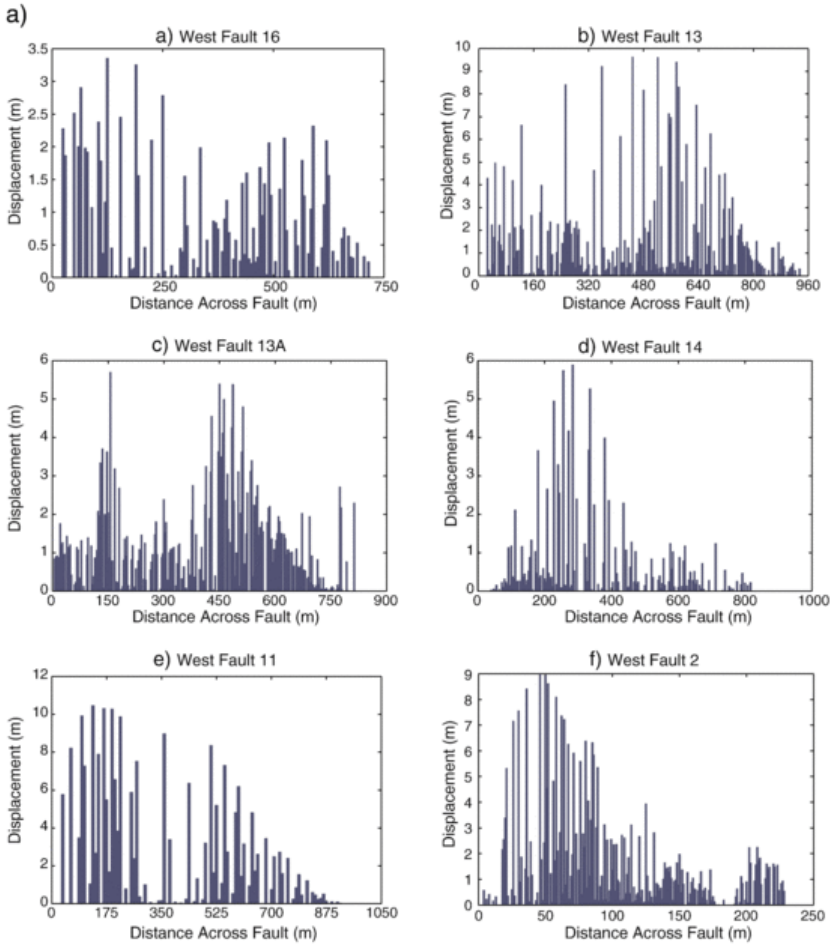

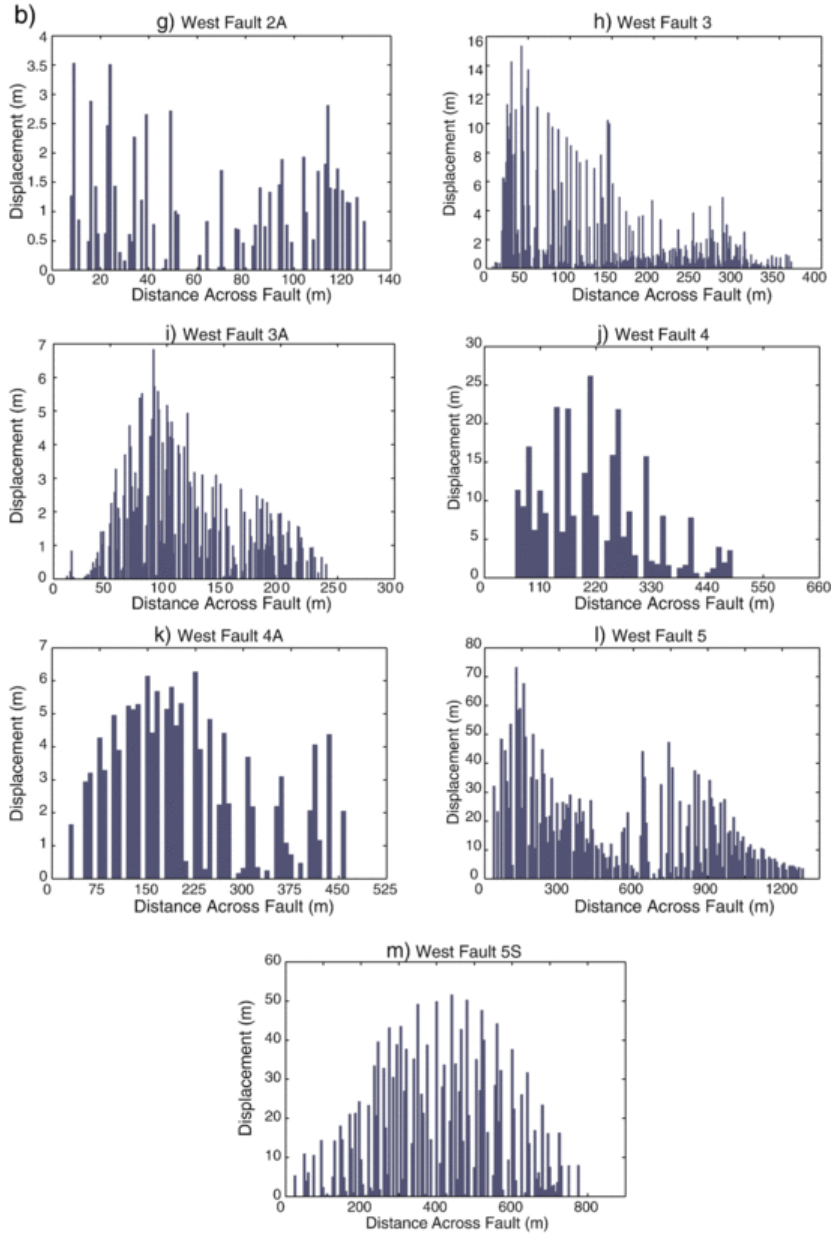

Fig. 7 Fault displacements for each of the 13 normal faults at Hail Creek as measured from the south westernmost point of each fault. All values from across the entire surface of each fault is shown, leading to large variations in adjacent displacements. Single, double and skewed displacement maxima are visible. Dashed lines indicate displacements constrained by modelling.

5 Fault system description

5.1 Fault groups and displacement profiles

The normal faults are clustered into four groups (Fig. 3). West Faults 13, 13A and 14 constitute the northern group, West Faults 2, 2A, 3 and 3A are in the centre of the study area, West Faults 4 and 4A occur towards the south, and West Faults 5 and 5S form the southernmost group. Within the fault groups, pairs of faults can be identified that generally dip towards each other, for example West Faults 2 and 3, 2A and 3A, and 13 and 14. In other cases the second fault is a synthetically dipping splay fault. This is apparent for West Faults 5 and 5S, and for 13 and 13A. West Faults 4 and 4A dip away from each other.

Displacement profiles of faults within the groups have been measured from a common origin at the southwest end of each fault group to show possible correspondence in displacement variations (Fig. 8). In the northernmost group of faults (Fig. 8a), West Faults 13 and 14 have asymmetric displacement profiles with steeper gradients on the SW side. Both of these faults have a displacement peak at around 250 m, which gives a strong combined displacement maximum in this position. Displacement on West Fault 13A increases as the displacement of the other two faults decreases.

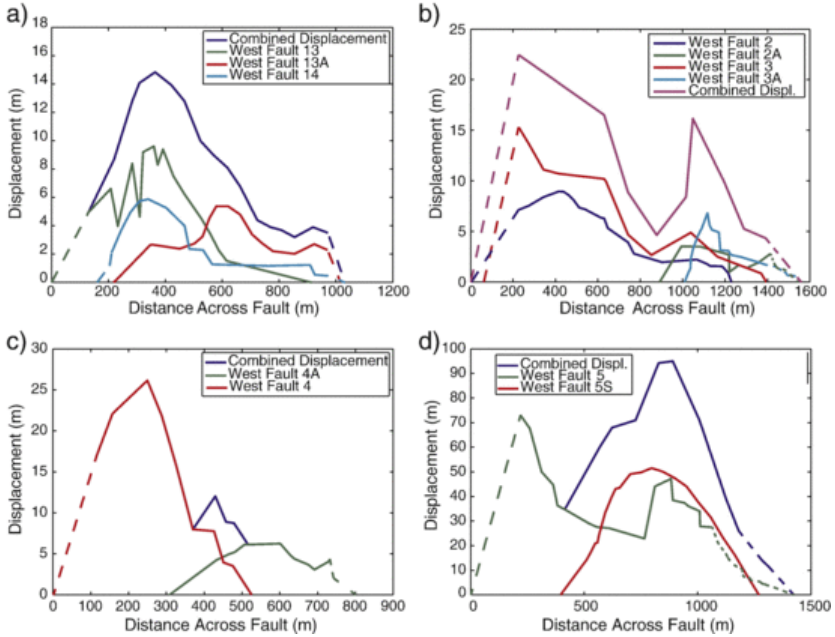

Fig. 8 Displacement profiles for individual faults within fault groups. The combined (aggregated) displacement reflects the degree of kinematic coherence of the group, but is not the total displacement because faults dip in opposite directions. The groups of faults from north to south are: (a) WFLT13, 13A and 14, (b) WFLT2, 2A, 3, 3A, (c) WFLT4 and 4A, and (d) WFLT5 and 5S.

The displacement profiles of faults in the West Fault 2, 2A, 3 and 3A group have single peaks, double peaks, and skewed geometries (Fig. 8b). West faults 2 and 3 have displacement peaks at approximately 350 m. Another set of coincident peaks for West Faults 2A, 3A and 3 is located at approximately 1100 m.

In the group comprised by West Fault 4 and 4A, the displacement maxima for the individual faults are complementary (Fig. 8c), but there is a substantial displacement deficit in the combined profile. In the southernmost group of faults, West Fault 5 has a double peak profile whilst West Fault 5S has a bell shaped profile. The displacement maxima of West Fault 5S correlates with the easternmost peak of West Fault 5. The resulting displacement aggregate is a double peaked bell curve.

Two patterns emerge from considering the displacement profiles of adjacent faults within the fault groups. In many cases there are coincident displacement peaks. Alternatively, displacement deficits (minima) on some faults occur at the positions of displacement peaks on others.

5.2 Displacement–length scaling

The fault models yield estimates of maximum displacement and length. Many similar data sets in the literature yield estimates of displacement restricted to 2-dimensional fault traces, but this limitation does not apply in the case of the Hail Creek 3-dimensional model. The Hail Creek data are comparable to the data sets analysed by Kim and Sanderson (2005), and supplement these data with relatively large displacement and length measurements (Fig. 9; Table 2). However, the constraints on the fault geometry need to be considered in order to understand the significance of this plot. Three faults (West Faults 4, 2, and 11) have their tip lines constrained by drilling, fault intersection or modelling at both ends, for which displacement–length scaling can be directly inferred (Fig. 10). These faults plot close to the normal fault fitting line from Kim and Sanderson (2005). The other faults are constrained only at one end, except for West Fault 5 that has no constraints at either end (Fig. 10). A lack of drilling data means that the NE tip line of most faults

is unconstrained (Fig. 10). The partially constrained faults (West Faults 2A, 3, 3A 4A, 5S, 13, 13A and 14), plot well within an order of magnitude of the displacement versus length line of Kim and Sanderson (2005).

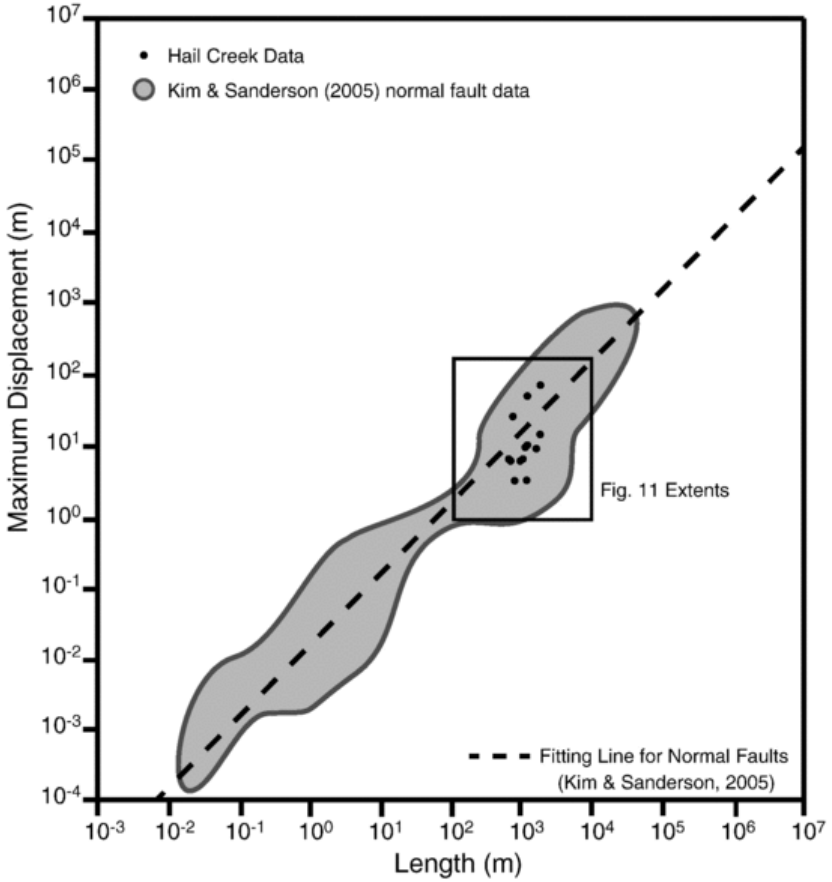

Fig. 9 Relation between maximum displacement and length for normal faults. The maximum displacement and length data for Hail Creek ~~is~~ are plotted as points and compared to ~~against~~ other data sets in the literature as summarised by the data compilation in Kim and Sanderson (2005). The Hail Creek measurements fall within the range of existing data, and represent large displacement and length values relative to the whole data set.

Table 2 Fault dimensions from the fault model.

Fault	Length, m	Maximum displacement, m	Average displacement, m
WFLT5	1488	73	17.7
WFLT5 Splay	1002	52	16.1
WFLT4A	581	6	3.2
WFLT4	622	26	8.5
WFLT12	2014	3	1.2
WFLT3	1406	15	4.1
WFLT3A	561	7	3.7

WFLT2	1220	9	3.4
WFLT2A	702	4	6.6
WFLT11	984	10	2.9
WFLT14	873	7	1.5
WFLT13A	803	7	0.2
WFLT13	971	10	4.9
WFLT16	977	3	1.0

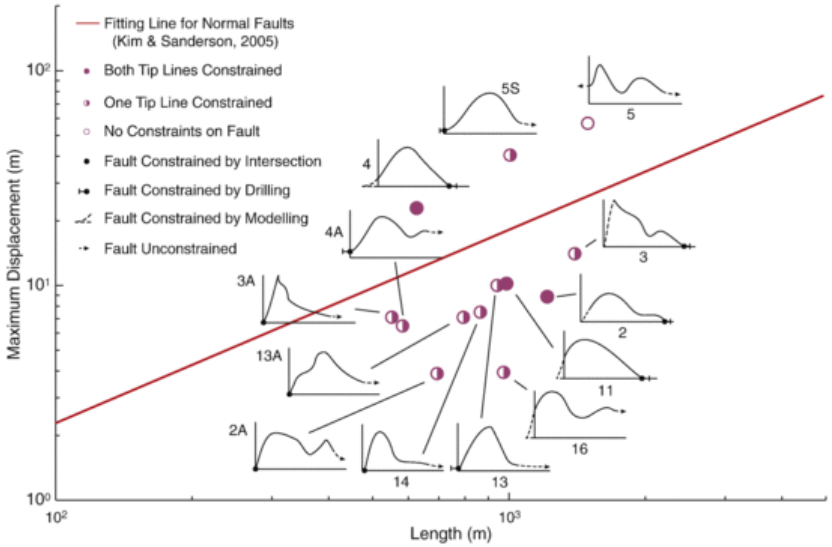

Fig. 10 Detailed maximum displacement–length scaling plot for faults at Hail Creek. Coloured symbols indicate constraints on fault tips: both tips (solid circle), one tip (half circle) or neither fault tip (open circle). The fault displacement profiles are shown schematically for each fault, with fault lengths normalised to a single length. The fault lengths are constrained by intersection, drilling, modelling or are unconstrained: these are shown as appropriate symbols on the schematic profiles.

5.3 Fault system orientations and kinematics

The orientations of the 13 normal faults and the triangles that comprise their surfaces are shown in Fig. 11. The individual faults dip to the NNW, SSE, NW and SE in four separate orientations, typical of an orthorhombic fault system. The triangles have a similar four-fold grouping, and show variable orientations within each group, with some triangles plotting in different fault sets.

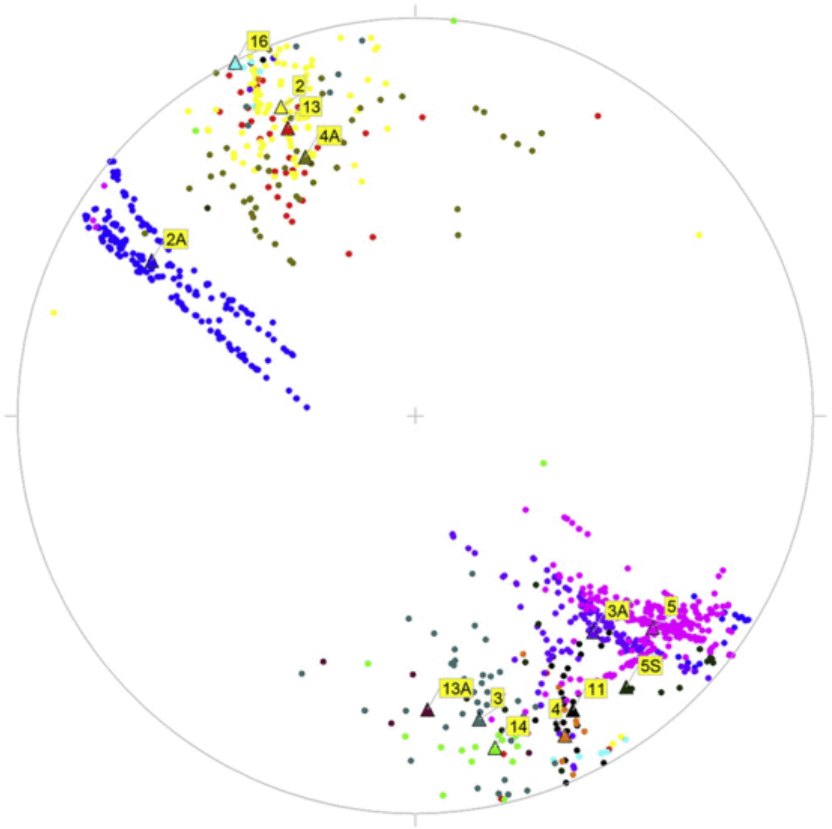

Fig. 11 Lower hemisphere, equal area stereoplot of poles to triangles on the 13 normal faults, with faults distinguished by colour. Triangles are the best fits.

The odd-axis technique has been applied in three different ways in order to analyse the kinematics of the Hail Creek faults at different scales. The methods are designated: (i) the identity method, (ii) the triangle method, and (iii) the cluster method. The identity method, which was used by Krantz (1988), who developed the odd-axis technique, uses an average dip and dip direction for the entire surface of each fault (Fig. 12a). In an orthorhombic fault system, this results in four clusters of poles to faults, from which a best-fit pole to each fault set is calculated. A great circle containing both the best-fit pole to the faults and the slip vector for each cluster is then drawn (Fig. 12a). The odd-axis is the best fit to the intersections of the four great circles. The odd-axis for normal faults is the minimum principal extension direction (ε_z) which plunges vertically. The intermediate (ε_y) and similar (ε_x) axes are found as the ~~acute~~obtuse and ~~obtuse~~acute bisectors of the intersections of the pairs of great circles on the plane perpendicular to the odd axis (Fig. 12a; cf. Krantz, 1988).

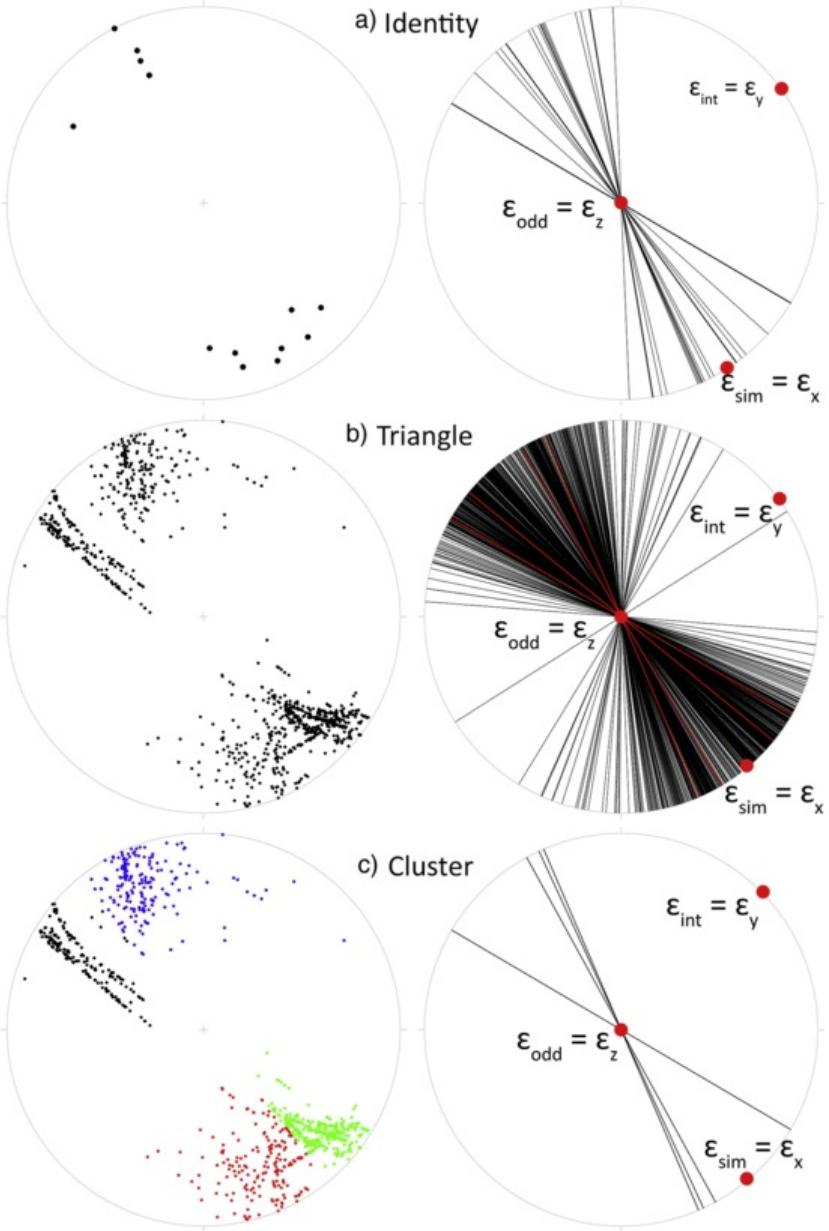

Fig. 12 Odd axis constructions for the identity (a), triangle (b) and cluster (c) methods. Equal area, lower hemisphere stereoplots of poles to faults (left) and great circles connecting fault poles and slip vectors, with the odd axis (ε_z, centre of net), the acute bisector (ε_x) and obtuse bisector (ε_y) of the great circles (right). All three methods give very similar orientations for the principal strains.

The odd-axis construction can also be performed using subsets of data from the fault surface, rather than taking an average strike and dip for each fault, thus investigating the kinematics at a more detailed scale. This concept has been implemented by the triangle method, which differs from the identity method by using the poles to every triangle of the fault surface. Fig. 12b shows the poles for each triangle in every fault. Great circles that connect each pole to its respective slip vector are plotted (Fig. 12b). Four great

circles are found by calculating the vector mean of the groups of poles to the great circles. As with the identity method, the intermediate and similar axes are calculated by finding the ~~acute~~obtuse and ~~obtuse~~acute bisectors of pairs of great circles on the plane normal to the odd axis.

In the final method, kinematics of the fault triangles are ~~is~~ investigated without regard to the location of the triangles. This cluster method of construction groups the poles to triangles into four clusters based on their orientation, ignoring their fault affiliation (Fig. 12c). The average pole to the fault of each cluster and the slip vector define~~s~~ the four great circles. The intermediate and similar axes are calculated in a similar fashion to the previous methods. The result of this construction allows a comparison between the kinematics of individual fault components to the whole system, as shown by the identity and triangle methods.

Table 3 shows the results of kinematic analysis produced from the three methods described above. The maximum principal strain ε_X given by all three methods is between SE and SSE. The orientations of the principal strains for the ~~i~~dentity and triangle methods differ by 2°. The results from the cluster method are within 9° of the other two (Table 3). The values of α, the angular separation of the families of great circles in the odd axis construction, are quite similar between the three methods, giving similar maximum strain ratios $\varepsilon_X/\varepsilon_Z$ (ca. ~~–~~ – 0.9). There is more variability in the other strain ratios (Table 3).

Table 3 Azimuths for the principal strains (ε_X, ε_Y~~)~~), α values, and principal strain ratios from the odd axis construction using the Identity, Triangle and Cluster methods.

	Identity	Triangle	Cluster
Azimuth of ε_x	148	146	139
Azimuth of ε_y	58	56	49
α	20.75	26.75	18.15
$\varepsilon_Y/\varepsilon_X$	0.062	0.25	0.11
$\varepsilon_Y/\varepsilon_Z$	– 0.058	– 0.20	– 0.097
$\varepsilon_X/\varepsilon_Z$	– 0.94	– 0.80	– 0.90

6 Discussion

6.1 ~~Displacement~~ Displacement–length scaling relationships of polymodal fault sets

The displacement~~–~~–length scaling for all the faults studied at Hail Creek ~~plot~~ plots within the envelope of global data for normal faults by Kim and Sanderson (2005). Even the data from the partially constrained faults plot near the Kim and Sanderson line, which may indicate that their true lengths and displacements are no more than an order of magnitude different from their observed values. The polymodal faults at Hail Creek therefore appear to have similar scaling relationships to other normal faults within the resolution of the data. The geometry of polymodal systems is more complex than single or conjugate fault sets, which might result in different fault interactions; even if this has occurred, the polymodal faults in this study have evolved to similar displacement~~–~~–length properties as other faults.

6.2 Kinematic coherence of polymodal fault sets

Kinematic coherence of faults implies that fault displacement profiles evolve in a linked fashion, leading ultimately to an aggregate displacement profile like a single structure with one, central displacement maximum (Nicol et al., 2010; Walsh and Watterson, 1991). The coincidence of displacement peaks on faults within the same group (e.g. West Faults 13, 13A and 14 in the northern group, Fig. 8a), suggests that these faults evolved within the same strain state and generally in the same deformation event. Likewise, the occurrence of displacement minima on some faults with displacement peaks on others in the same group (e.g. West Faults in the group containing West Faults 2, 3, 2A and 3A; Fig. 8b) suggests a complementary pattern that is evidence for kinematic coherence.

Each combined displacement profile shows a major peak with subsidiary peaks (Fig. 8). This suggests that none of the fault groups have achieved full kinematic coherence, despite the evidence for linked evolution of the faults in each group. It is possible that this is a characteristic of aggregated displacement profiles of polymodal fault sets. The multiple orientations of the faults may preclude the system from evolving to a single approximately planar structure with a unified displacement profile, as in the case of approximately parallel faults (e.g. Anders and Schlische, 1994; Dawers and Anders, ~~2004~~1995; Nicol et al., 2005).

6.3 Evolution of polymodal fault sets

The four orientations of faults and fault components (as represented by triangles) at Hail Creek ~~is~~ are a typical configuration for an orthorhombic, polymodal fault system. There is no evidence for consistent cross-cutting relationships between these faults, and

their common characteristics and kinematic coherence strongly suggest that the fault system evolved in a single deformation event.

The orientations of the faults and fault components hint at the way in which the fault system may have evolved. The individual faults are comprised of components in a variety of orientations (Fig. 11). At least two factors appear to be important in determining component orientation. Much of the variation in the dip of triangle orientation is attributable to lithology (Fig. 5a). The decrease in dip angle from sandstone to siltstone to ~~clay~~mudstone to coal and tuff correspond~~s~~ to changes in relative strengths of these rocks and has a simple explanation in terms of a typical failure envelop on a Mohr diagram (Fig. 5b). For stronger rocks with steeper failure envelops, larger angles are predicted between the normal to the failure plane and the maximum principal stress (e.g. Jaeger and Cook, 1979). For a vertical maximum principal stress, this will result in larger dip angles. Fig. 5b is not meant to imply failure according to any particular criterion: no general stress-based failure criterion has been satisfactorily proven for polymodal faults.

However, not all of the variation in the orientation of fault surface components is due to dip change. Fault surfaces comprise components that vary in dip direction, as well as magnitude of dip (Fig. 11), with a range of dip directions similar to the range of the polymodal fault orientations (~ 20°: Fig. 11). West Faults 2, 4A, 5, and 11 even include components with the orientations of different fault sets (Fig. 11). Dip direction reversals may occur between components of individual faults (Fig. 5f; Fig. 11). This variability suggests that the faults ~~are~~ formed by the propagation or linkage of components in a range of orientations (Fig. 13). The horizontal scale of resolution of the fault displacements (tens of m) is not sufficient to resolve further details of fault evolution at this scale. However the existence of two peak displacements (e.g. West Faults 3, 5, and 13A: Fig. 8) suggests that some faults may have formed by the linkage of segments from one to several hundred m in length.

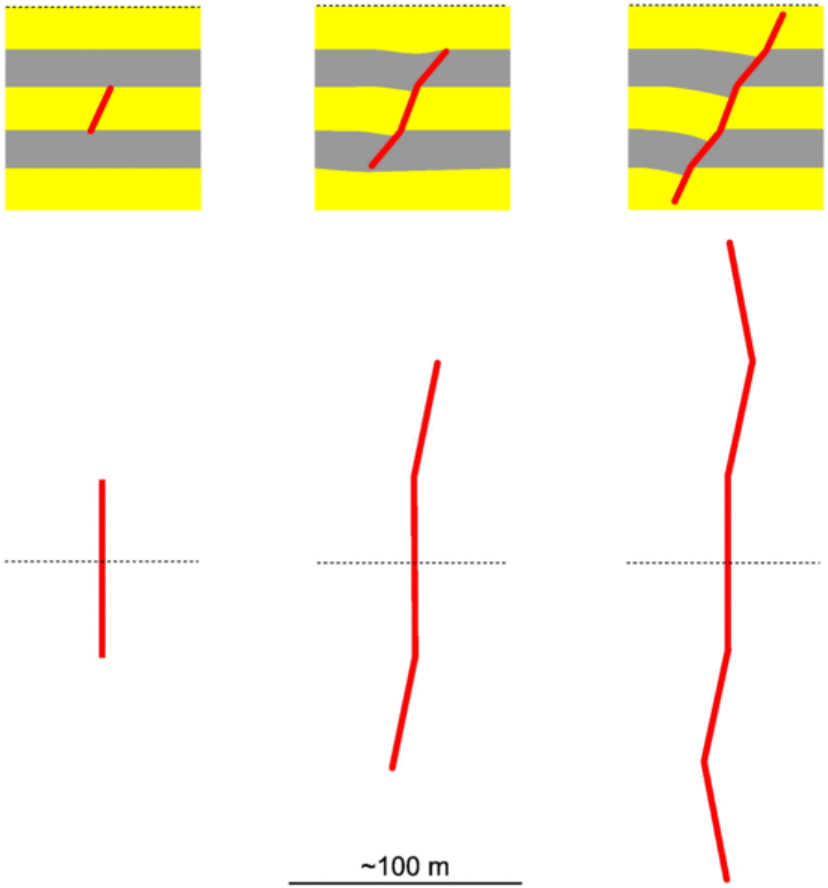

Fig. 13 Possible evolution of a polymodal fault in cross section (top) and map view by propagation or linkage in variable orientations, suggested by the variability in fault component orientation shown in Fig. 12. Yellow and grey layers represent more and less competent units respectively. (For interpretation of the references to colour in this figure legend, the reader is referred to the web version of this article.)

The coincidence between the odd-axis constructions for the individual fault triangles (triangle method), for the whole fault surface (identity method), and for the aggregates of the triangles (cluster method) reinforces the idea that the fault system evolved as a coherent, polymodal system from the early stages. The identity method for the odd axis construction, the classical method proposed by Krantz (1988), provides a standard to compare with the other methods. Krantz (1988) had limited data for individual fault surfaces

compared to what is available at Hail Creek, where applying this method has the effect of averaging all the data, and examining the kinematics of the faults on a broad scale. The triangle and cluster methods incorporate all of the data points and thus examine kinematics at a more detailed scale. The results from all three methods are very similar, and indicate that the polymodal fault system is formed in response to triaxial strain, consisting of vertical shortening and two directions of horizontal lengthening, the greatest being between SE and SSE.

The large-scale features of the orthorhombic fault system at Hail Creek described here are similar other polymodal systems (e.g. Aydin and Reches, 1982; Reches, 1978), but details of fault surfaces and displacement distributions in these systems have not been described before. It is possible that the geometries, kinematics and evolution of the Hail Creek faults may be more generally applicable to polymodal systems.

7 Conclusions

Faults at Hail Creek coal form a polymodal fault system. Detailed mapping and modelling as the faults have been exposed by mining allow the kinematics and evolution of this orthorhombic fault system to be analysed. The faults are arranged in four groups of closely spaced faults. They have the same displacement scaling laws as other normal faults, despite potentially more complex interactions because of their geometry. Displacement exchange occurred between faults, so that faults within groups display a degree of kinematic coherence on a scale of one hundred to several hundred metres. Fault orientations were influenced by lithology, with steeper fault dips occurring in more competent units. The fault system evolved by the propagation or linkage of components with a similar range of orientations to the larger scale polymodal system. Fault linkage occurred between segments on a larger scale of hundreds of metres. The system formed in response to triaxial strain with a maximum extension orientated between SE and ESE throughout its history.

8 Uncited reference

Walsh et al., 1991

AcknowledgmentsAcknowledgements

We are grateful to the staff of Hail Creek Mine for their assistance, and to the helpful journal reviews by Ze'ev Reches and Hengmao Tong.

References

Alves T.M., Scale-relationships and geometry of normal faults reactivated during gravitational gliding of Albian rafts (Espírito Santo Basin, SE Brazil), *Earth Planet. Sci. Lett.* **331–332**, 2012, 80–96.

Anders M.H. and Schlische R.W., Overlapping faults, intrabasin highs, and the growth of normal faults, *J. Geol.* **102**, 1994, 165–179.

Anderson E.M., The Dynamics of Faulting and Dyke Formation With Applications to Britain, 1951, Oliver and Boyd; Edinburgh.

Arthaud F., Méthode de détermination graphique des directions de raccourcissement, d'allongement et intermédiaire d'une population des failles, *Bull. Soc. Géol. France* **7** (11), 1969, 729–737.

Aydin A. and Reches Z., Number and orientation of fault sets in the field and in experiments, *Geology* **10** (2), 1982, 107–112.

Barnett J.A.M., Mortimer J., Rippon J.H., Walsh J.J. and Watterson J., Displacement geometry in the volume containing a single normal fault, *Am. Assoc. Pet. Geol. Bull.* **71**, 1987, 925–937.

Bowring S.A., Erwin D.H., Jin Y.G., Martin M.W., Davidek K. and Wang W., U/Pb zircon geochronology and tempo of the end-Permian mass extinction, *Science* **280** (5366), 1998, 1039–1045.

Cartwright J.A., Trudgill B.D. and Mansfield C.S., Fault growth by segment linkage: an explanation for scatter in maximum displacement and trace length data from the Canyonlands Grabens of SE Utah, *J. Struct. Geol.* **17** (9), 1995, 1319–1326.

Cladouhos T.T. and Marrett R.A., Are fault growth and linkage models consistent with power-law distributions of fault length, *J. Struct. Geol.* **18**, 1996, 281–294.

Clark R.M. and Cox S.J.D., A modern regression approach to determining fault displacement–length scaling relationships, *J. Struct. Geol.* **18**, 1996, 147–154.

Cowie P.A. and Scholz C.H., Growth of faults by accumulation of seismic slip, *J. Geophys. Res.* **97**, 1992a, 11,085–11,095.

Cowie P.A. and Scholz C.H., Physical explanation for the displacement–length relationship of faults using a post-yield fracture mechanics model, *J. Struct. Geol.* **14** (10), 1992b, 1133–1148.

Dawers N.H. and Anders M.H., Displacement–length scaling and fault linkage, *J. Struct. Geol.* **17** (5), 1995, 607–609.

Dawers N.H., Anders M.H. and Scholz C.H., Growth of normal faults: displacement–length scaling, *Geology* **21** (12), 1993, 1107–1110.

Esterle J.S., Sliwa R., Smith L.G., Vincent J.R., Williams R., et al., Bowen Basin Supermodel 2000, 2002, CSIRO Exploration & Mining; Kenmore, Qld.

Finlayson ~~D. M.~~D.M., The Eromanga–Brisbane Geoscience Transect: A Guide to Basin Development Across Phanerozoic Australia in Southern Queensland, In: *Geology of Australia,* 1990, Geoscience Australia.

Healy D., Jones R.R. and Holdsworth R.E., Three-dimensional brittle shear fracturing by tensile crack interaction, *Nature (London)* **439**, 2006a, 64–67.

Healy D., Jones R. and Holdsworth R., New insights into the development of brittle shear fractures from a 3-D numerical model of microcrack interaction, *Earth Planet. Sci. Lett.* **249**, 2006b, 14–28.

Jaeger J.C. and Cook N.G.W., Fundamentals of Rock Mechanics, 3rd ed., 1979, Chapman and Hall; London.

Kim Y. and Sanderson D.J., The relationship between displacement and length of faults: a review, *Earth Sci. Rev.* **68** (3–4), 2005, 317–334.

Korsch R.J., Wake-Dyster K.D. and Johnstone D.W., Seismic imaging of Late Palaeozoic—Early Mesozoic extensional and contractional structures in the Bowen and Surat basins, eastern Australia, *Tectonophysics* **215** (3–4), 1992, 273–294.

Korsch R.J., Totterdell J.M., Fomin T. and Nicoll M.G., Contractional structures and deformational events in the Bowen, Gunnedah and Surat Basins, eastern Australia, *Aust. J. Earth Sci.* **56** (3), 2009, 477–499.

Krantz R.W., Multiple fault sets and three-dimensional strain~~;~~: theory and application, *J. Struct. Geol.* **10** (3), 1988, 225–237.

Mallet C.W., McLennan T., Balfe P. and Sullivan D., Bowen Basin, In: Ward C.R., Mallet C.W. and Beeston J.W., (Eds.), *Geology of Australian Coal Basins, Geological Society of Australia, Coal Geology Group* **vol. 1**, 1995, 299–340.

Malone, E.J., Corbett, D., Jensen, A.R., 1991. Geology of the Mount Coolon 1:250,000 sheet area. Dept. of National Development, Bureau of Mineral Resources, Geology and Geophysics.

Marrett R. and Allmendinger R.W., Estimates of strain due to brittle faulting: sampling of fault populations, *J. Struct. Geol.* **13**, 1991, 735–738.

Michaelsen P. and Henderson R.A., Facies relationships and cyclicity of high-latitude, Late Permian coal measures, Bowen Basin, Australia, *Int. J. Coal Geol.* **44** (1), 2000, 19–48.

Muraoka H. and Kamata H., Displacement distribution along minor fault traces, *J. Struct. Geol.* **5** (5), 1983, 483–495.

Nicol A., Watterson J., Walsh J.J. and Childs S., The shapes, major axis orientations, and displacement patterns of fault surfaces, *J. Struct. Geol.* **18**, 1996, 235–248.

Nicol A., Walsh J., Berrymana K. and Nodder S., Growth of a normal fault by the accumulation of slip over millions of years, *J. Struct. Geol.* **27**, 2005, 327–342.

Nicol ~~A~~A., Walsh ~~J. J.~~J.J., Villamor P., Seebeck H. and Berryman ~~K. R.~~K.R., Normal fault interactions, paleoearthquakes and growth in an active rift, *J. Struct. Geol.* **32** (8), 2010, 1101–1113.

Oertel G., The mechanism of faulting in clay experiments, *Tectonophysics* **2**, 1965, 343–393.

Peacock D.C.P., Propagation, interaction and linkage in normal fault systems, *Earth Sci. Rev.* **58** (1–2), 2002, 121–142.

Peacock D.C.P. and Sanderson D.J., Displacements, segment linkage, and relay ramps in normal fault zones, *J. Struct. Geol.* **13**, 1991, 721–733.

Reches Z., Analysis of faulting in three-dimensional strain field, *Tectonophysics* **47** (1–2), 1978, 109–129.

Reches Z., Faulting of rocks in three-dimensional strain fields~~:~~ II~~–~~, Theoretical analysis, *Tectonophysics* **95** (1–2), 1983, 133–156.

Reches Z. and Dieterich J.H., Faulting of rocks in three-dimensional strain fields~~:~~ I~~–~~, Failure of rocks in polyaxial, servo-control experiments, *Tectonophysics* **95** (1–2), 1983, 11–132.

Schilsche R.W., Structural and stratigraphic development of the Newark extensional basin, eastern North America: evidence for the growth of the basin and its bounding structures, *Geol. Soc. Am. Bull.* **104** (10), 1992, 1246–1263.

Sutherland F.L., Mesozoic–Cainozoic volcanism of Australia, *Tectonophysics* **48** (3–4), 1978, 413–427, DOI: 10.1016/0040-1951(78)90126-9.

Walsh J.J. and Watterson J., Distributions of cumulative displacement and seismic slip on a single normal fault surface, *J. Struct. Geol.* **9** (8), 1987, 1039–1046.

Walsh J.J. and Watterson J., Geometric and Kinematic Coherence and Scale Effects in Normal Fault Systems, In: Roberts A.M., Yielding G. and Freeman B., (Eds.), *The Geometry of Normal Faults, Geological Society London Special Publication* **56**, 1991, 193–203.

Walsh J. and Watterson J., Geometric and kinematic coherence and scale effects in normal fault systems, *Geol. Soc. Lond., Spec. Publ.* **56**, 2002, 193–203.

Walsh J., Watterson J. and Yielding G., The importance of small-scale faulting in regional extension, *Nature (London)* **351** (6325), 1991, 391–393.

Walsh J.J., Nicol A. and Childs C., An alternative model for the growth of faults, *J. Struct. Geol.* **24** (11), 2002, 1669–1675.

Watterson J., Fault dimensions, displacements and growth, *Pure Appl. Geophys.* **124** (1–2), 1986, 365–373.

Graphical abstract

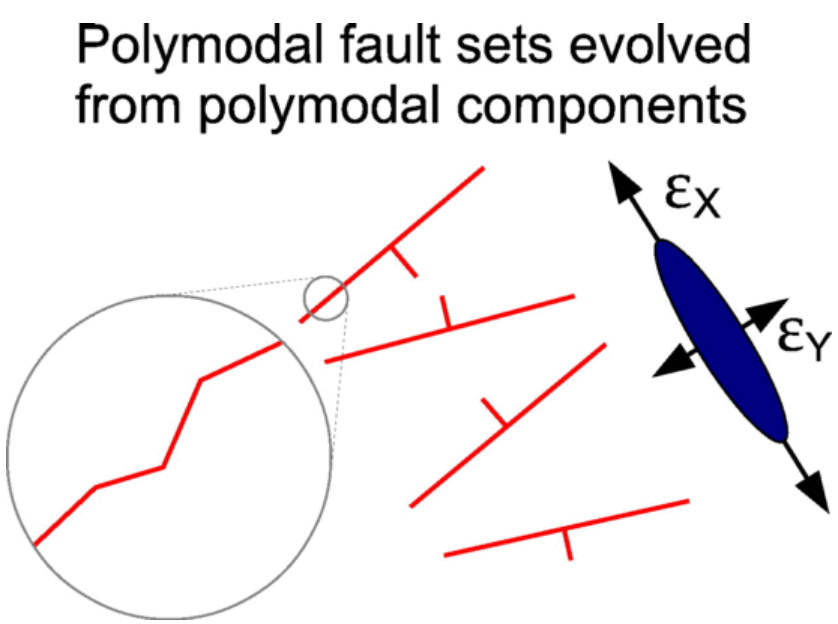

Highlights

- Coal seems seams are cut by normal faults in an orthorhombic network.
- The polymodal faults have typical displacement–length ratios for normal faults.
- Faults are kinematically coherent in groups.
- Faults evolved by growth of variably orientated components.

Queries and Answers

Query:

Please confirm that given names and surnames have been identified correctly.

Answer: Yes, they are correct

Query:

The citation “Cowie and Scholz, 1992” has been changed to match the author name/date in the reference list. Please check here and in subsequent occurrences, and correct if necessary.

Answer: OK

Query:

The citation “Walsh and Watterson, 1988” has been changed to match the author name/date in the reference list. Please check here and in subsequent occurrences, and correct if necessary.

Answer: OK

Query:

The citation “Michaelsen et al., 2000” has been changed to match the author name/date in the reference list. Please check here and in subsequent occurrences, and correct if necessary.

Answer: OK

Query:

The citation “Michaelsen et al., 2000” has been changed to match the author name/date in the reference list. Please check here and in subsequent occurrences, and correct if necessary.

Answer: OK

Query:

The citation “Michaelsen et al., 2000” has been changed to match the author name/date in the reference list. Please check here and in subsequent occurrences, and correct if necessary.

Answer: OK

Query:

This sentence has been slightly modified for clarity. Please check that the meaning is still correct, and amend if necessary.

Answer: OK

Query:

Citation “Dawers and Anders, 2004” has not been found in the reference list. Please supply full details for this reference.

Answer: Should be Dawers and Anders, 1995

Query:

This sentence has been slightly modified for clarity. Please check that the meaning is still correct, and amend if necessary.

Answer: OK

Query:

This sentence has been slightly modified for clarity. Please check that the meaning is still correct, and amend if necessary.

ELSEVIER_TECTO_126344

Answer: Delete the "is". These events happened in the past

Query:

Uncited reference: This section comprises references that occur in the reference list but not in the body of the text. Please position each reference in the text or, alternatively, delete it. Thank you.

Answer: Delete this reference